THE JOURNAL OF PHYSICAL CHEMISTRY A

pubs.acs.org/JPCA Article

Positron Scattering from Pyridine and Pyrimidine

Nidhi Sinha, Aloka Kumar Sahoo, and Bobby Antony*

Cite This: J. Phys. Chem. A 2020, 124, 5147−5156 Read Online

ACCESS | Metrics & More | Article Recommendations

ABSTRACT: Positron impact scattering cross-sections for pyridine and pyrimidine are reported here. Spherical complex optical potential formalism is used to calculate the positronium formation, elastic, total, and differential cross-sections. The ionization cross-sections calculated here are obtained employing the complex scattering potential—ionization contribution method. To account for the complex molecular structure of the target, an effective potential method is employed in our formalism for the first time. The contribution from rotational excitation is also included, which shows a reasonable comparison with the experimental data. The results obtained using the modified approach are encouraging and show very good agreement with the measurements. The differential cross-section for pyridine is reported for the first time.

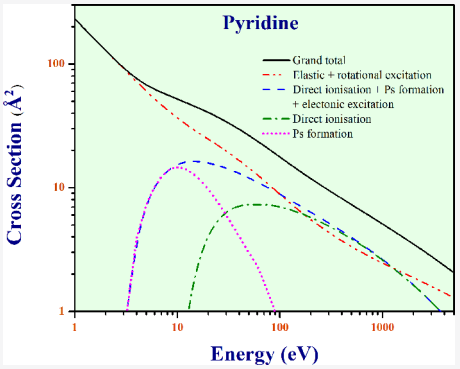

INTRODUCTION

Pyridine is a simple aromatic heterocyclic organic compound with the molecular formula C_5H_5N (Figure 1). It comprises a

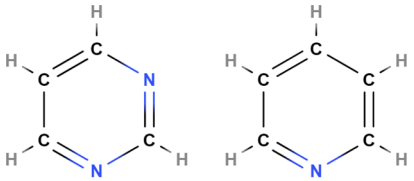

Figure 1. Molecular structure of the present targets.

core benzene ring with one methine group being replaced by a nitrogen atom. This azarene is the parent molecule for a class of compounds named pyridines. Pyridine and its derivatives are very important in the medical field.[1] Pyridine nucleotides are found in vitamin B series and nicotine[2] and further have principal contribution in treating cardiovascular diseases.[3] Moreover, pyridine derivatives have medicinal properties like antidiabetic, antioxidant, etc.[4] Chemicals based on these compounds play a major role in the preparation of pesticides[5,6] as well. Furthermore, pyridine carboxylic and dicarboxylic acids were found in a number of CM2 carbonaceous chondrites[7,8] (meteorites containing a considerable amount of organic carbon), which implicates the formation of pyridine in the interstellar medium[9] and makes it important to study its interaction with various atomic and subatomic particles. Furthermore, being an important biomolecule, pyridine interaction with positrons is of special interest apropos to positron emission tomography (PET) scans.[10,11] Using positron emitters in PET scans has aided the early detection of cancer and brain disorders. Furthermore, this technique has also been considered as an alternative to ion beam cancer treatments for dosimetry purposes. The cross-section resulting from the interaction of positrons with biologically relevant media is used to model single positron tracks in such media.[12] Like pyridine, another biomolecule relevant to such studies is pyrimidine ($C_4H_4N_2$).[13] Pyrimidine-specific chemical reactions are useful for DNA sequencing.[14] Hence, in this article, we focus on the theoretical calculation of various positron impact cross-sections for pyridine and pyrimidine, which will be of use in Monte-Carlo simulation codes. The particle-tracking codes[15] such as PENELOPE, GEANT, and LEPTS are used to model the radiation damage at the cellular level, which require cross-sections as their basic input.

Zecca et al.[16] reported the first experimental total cross-sections for pyrimidine in the energy range of 0.3−45 eV. They also performed theoretical calculations under the framework of an independent atom model with the screening-corrected additivity rule (IAM-SCAR). They reported theoretical cross-sections, which include the contribution from rotational excitation as well. Palihawadana et al.[17] reported a range of cross-sections including positronium formation, differential elastic, total elastic, and grand total cross-sections. On the theoretical front, the spherical complex optical potential

Received: March 24, 2020
Revised: June 2, 2020
Published: June 2, 2020

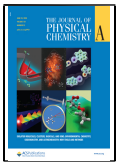

https://dx.doi.org/10.1021/acs.jpca.0c02575
J. Phys. Chem. A 2020, 124, 5147−5156

(SCOP) results of Sinha and Antony,[18] Schwinger multichannel calculation (SMC) of Barbosa et al.,[19] the *R*-matrix and IAM results of Sanz et al.,[20] and a quantum mechanical approach of Franz and Gianturco[21] are also available. In addition, Franz and Gianturco used their theoretical DCS to determine the forward angle correction in two measurements, which are nearly equal in magnitude. Furthermore, these theoretical attempts are largely concentrated on the elastic process and no theoretical cross-section for ionization or positronium (Ps) formation is reported. In this article, we report the first theoretical cross-section for Ps formation for pyrimidine. Furthermore, it is the maiden attempt to report ionization and electronic excitation cross-sections. Very recently, cross-sections for pyridine were first reported by Stevens et al.[22] They reported a range of cross-sections, viz. elastic, inelastic, positronium formation, and total cross-sections. Along with the experiment, the IAM-SCAR including the interference effects (IAM-SCAR+I) was also used for the theoretical calculations. In this work, we employ the SCOP method[23] to compute the cross-sections from 1 to 5000 eV. To comprehend the molecular system, we apply a different approach, which we have named the "effective potential method" (EPM). This method is applied for the first time and will be discussed in the next section. The SCOP along with the EPM is used to calculate the differential and integral elastic, positronium formation, and total cross-sections. The complex scattering potential-ionization contribution (CSP-ic) method[23,24] is used to determine the direct ionization cross-section. Electronic excitation and total ionization cross-sections are also reported along with. Such a detailed study of cross-sections over the present energy range is one of a kind for pyridine molecules.

THEORETICAL METHODOLOGY

We have applied the SCOP method[24] to calculate the differential and integral cross-sections. Using this method, the interaction potential is represented in two parts: real and imaginary. Static (V_{st}) and polarization potentials (V_{pol}) contribute to the real part and the imaginary part accounts for the loss of flux because of various inelastic processes.

$$V_{opt} = V_R + V_I = V_{st} + V_{pol} + iV_{abs} \tag{1}$$

The potential arising because of the electric field of the undisturbed target charge cloud is termed as the static potential. It is represented as an analytic expression involving the sum of the Yukawa terms from the work of Salvat et al.[25] The final form is given as

$$V_{st} = \frac{Z}{r}\sum_{i=1}^{3} A_i\, e^{(-\alpha_i r)} \tag{2}$$

and the charge density (ρ) can then be derived as

$$\rho(r) = \frac{Z}{4\pi r}\sum_{i=1}^{3} A_i\alpha_i^2\, e^{(-\alpha_i r)} \tag{3}$$

where A_i and α_i are called the potential field parameters and determined using the least squares fit of radial electron density. Z and r are, respectively, the atomic number of the element and the radial distance. The values of A_i and α_i can be found in the article of Salvat et al.[25] To use these parameters for a molecular system, the following procedure is applied. If there is overlapping between the charge cloud of two atoms (CH in the present case), the single-center expansion technique is applied, where the parameters of Salvat et al.[25] are used as the input. In the single-center approach,[26] we take into account the bonding effect of constituent atoms of the molecule by considering a single scattering center. The total charge density and the static potential of the scattering centers are obtained as a function of radius from the center of mass of the two atoms considered. However, if there is no overlap, then the charge density and static potentials can be simply added, assuming that the atoms are independent of each other. Following this procedure, the charge density and static potential of nitrogen atoms are derived directly using the form given by Salvat et al.[25]

Polarization potential (V_{pol}) arises because of the transient redistribution of the charge cloud of the target atom/molecule because of the electric field of the approaching projectile producing dipole and quadrupole moments. There are different models describing the correlation−polarization potential. The polarization potential should approach the short-range correlation part V_{co} near the target region and a correct asymptotic form for large r. Zhang et al.[27] proposed such a form, mathematically written as

$$V_{pco} = \frac{-\alpha_d}{2(r^2 + r_{co}^{\ 2})^2} \tag{4}$$

where r_{co} can be determined by putting $V_{pco}(r) = \frac{-\alpha_d}{2r_{co}^{\ 4}} = V_{co}(r)$. This makes $V_{pco}(r)$ equal to $V_{co}(r)$ in the near target region and approaches the asymptotic form for large r. Here, α_d is the static dipole polarizability. We have used eq 4 for determining the polarization potential in our calculations.

For $V_{co}(r)$, the form given by Perdew and Zunger[28] is used.

$$V_{co}(r) = \begin{cases} 0.0311\ln(r_s) - 0.0584 + 0.00133r_s \\ \quad \ln(r_s) - 0.0084r_s, & r_s < 1 \\ \dfrac{\gamma\left(1 + \frac{7}{6}\beta_1 r_s^{1/2} + \frac{4}{3}\beta_2 r_s\right)}{(1 + \beta_1 r_s^{1/2} + \beta_2 r_s)^2}, & r_s \geq 1 \end{cases} \tag{5}$$

where the constants are $\gamma = -0.1423$, $\beta_1 = 1.0523$, and $\beta_2 = 0.3334$. $r_s = \sqrt[3]{\frac{3}{4\pi\rho(r)}}$ is the density parameter. Moreover, the calculation was tried using the positron correlation potential[29] as well. However, the level of agreement with the experiment was poor as compared to the electron correlation potential.

Absorption potential reported by Staszewska et al.[30] is modified to deal with positron scattering. The original model includes the exchange channel in the case of electron scattering. However, for positrons, there is no exchange and hence the original expression is multiplied by 2. Furthermore, Blanco and García[31] found that there was a mistake in the derivation of this absorption potential and the correction factor of 0.5 should be multiplied with the original form. They also introduced a correction factor taking care of e^-−e^- dispersion dominant in the low-energy region. However, because this is not applicable to positron scattering, we have excluded this correction term. Thus, the final formula that is used in the present work is given as,

https://dx.doi.org/10.1021/acs.jpca.0c02575
J. Phys. Chem. A 2020, 124, 5147−5156

$$V_{abs} = -\rho(r)\left[\sqrt{\frac{T_{loc}}{2}}\left(\frac{8\pi}{10{k_f}^3 E_i}\right)\theta(p^2 - {k_f}^2 - 2\Delta)\right.$$
$$\left.(A_1 + A_2 + A_3)\right] \quad (6)$$

where, $T_{loc} = E_i - (V_{st} + V_{pol})$ is the local kinetic energy of the incident positron. k_f is the fermi wave vector, $[3\pi^2\rho(r)]^{1/3}$, and $p(=\sqrt{2E})$ is the momentum of the positron. A_1, A_2, and A_3 are dynamic functions, which depend differently on the charge density $\rho(r)$, ionization potential, absorption threshold (Δ), and incident energy of positrons (E_i) and are given as

$$A_1 = \frac{5{k_f}^3}{2\Delta}, \qquad A_2 = -\frac{{k_f}^3(5p^2 - 3{k_f}^3)}{(p^2 - {k_f}^2)^2},$$
$$A_3 = 2\theta(2{k_f}^2 + 2\Delta - p^2)\frac{(2{k_f}^2 + 2\Delta - p^2)^{5/2}}{(p^2 - {k_f}^2)^2} \quad (7)$$

$\theta(x)$ is the Heaviside step-function, such that $\theta(x) = 1$ for $x \geq 0$ and zero otherwise. The parameter Δ determines the threshold energy for inelastic channels. For incident energies less than Δ, the inelastic channels are closed.

The key input for V_{abs} is the inelastic threshold. Most popular forms give a smooth variation of Δ from the Ps formation threshold (Δ_p) to electronic excitation threshold (Δ_e). This way, indirectly, the Ps formation channel is included in the theory. We have used the exponential form suggested by Chiari et al.[32] However, we made two major changes to this form though the basic formula remains the same as that of the original one. First, the equation given by Chiari et al.[32] is applicable for atoms and they have used the IAM to investigate positron-molecule interactions. Because the present theory is capable of including the geometry of the complex target, it is logical to use molecular target parameters extending the approach for studying positron-molecule scattering efficiently. Second, we found that using Δ_e in the formula gave high cross-sections for the elastic and total process and very low magnitude for the Ps formation cross-section. Because Δ_e and Δ_p are close to each other (Table 1), the form given by Chiari et al.[32] does not correctly represent the Ps formation channel. Hence, we have replaced Δ_e by the ionization energy (I) of the molecule. The form is mathematically written as

$$\Delta(E) = I - (I - \Delta_p)\exp\frac{-(E - \Delta_p)}{E_m} \quad (8)$$

Here E_m is the energy at which the inelastic cross-section reaches its maximum when calculated using $\Delta = I$ ($\Delta = \Delta_e$ in the original article). For both the targets, this energy was found to be around 60 eV. Thus, using eq 8 gives us the inelastic cross-section, which includes the Ps formation channel (Q_{inel}).

Table 1. Target Properties

property	pyrimidine	pyridine
ionization energy (eV)	9.33[33]	9.26[33]
positronium formation threshold (eV)	2.53	2.46
first electronic excitation threshold (eV)	4.0[34]	4.1[35]
static dipole polarizability (Å^3)	8.54[33]	9.493[33]
dipole moment (D)	2.334[20]	2.19[33]
C−H bond length (Å)	1.0831, 1.0833 (2), 1.0798[33]	1.0826 (2), 1.0865 (2), 1.0818[36]

Using EPM, the scattering centers present in the molecule are identified initially. For pyridine, six scattering centers were located; five CH and one N. Because the charge cloud of carbon and hydrogen atoms overlaps, CH is treated as one single center. This can be concluded by studying the bond length between different atoms of the molecules or by generating the potential energy surface via any available software. We have used AVOGADRO software[37] for this purpose and as can be seen from Figure 2, different scattering centers are easily separated from each other. Similarly, for pyrimidine, four CH and two N centers were located. As explained earlier, the charge density and static potential are computed for each scattering center. This charge density for each scattering center works as the input to model the polarization potential for that center. Clearly, r_{co} also differs for each scattering center. In the near target region, $(r \to 0)$ r_{co} is nearly equal to the radius of the scattering center, depending on the entity for which the polarization potential is calculated. For the present case, it was found to be around $3.8a_0$. This way potentials, namely static and polarization potentials, are calculated from each scattering center and these effective potentials are used to determine the local kinetic energy (T_{loc}) of the incident positron. Using the above threshold and effective potential, the Schrödinger equation is solved to obtain the phase shifts. These phase shifts are then used to compute the cross-sections for the molecule. Thus, rather than adding the cross-sections from different scattering centers, we have determined the effective potential that is generated by the molecule, which we believe is a better approach to study a molecular system. Henceforth, we call this approach the SCOP-EPM method. We will see in Results and Discussion that SCOP-EPM gives excellent results even at low energies, which we were struggling to produce earlier, especially for the differential cross-section.

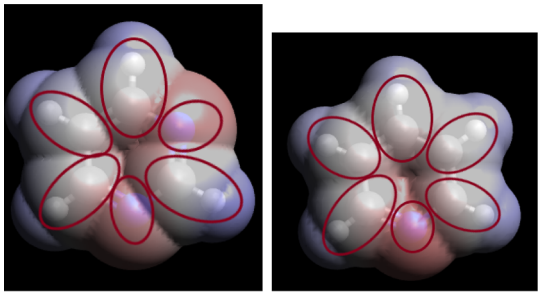

(a) Pyrimidine (b) Pyridine

Figure 2. Potential energy surface generated to identify scattering centers.

To determine the direct ionization cross-section, we apply the modified form of the CSP-ic method.[24] It is fundamentally a ratio-driven method, where $R = Q_{ion}/Q_{in}$. $Q_{in}(Q_{ion} + Q_{elec,exc})$ is the inelastic cross-section excluding the Ps formation channel. To obtain this cross-section, we have used $\Delta = 0.8I + \beta(E - I)$ in our codes. β can be determined by equating $\Delta = I$ when $E = E_m$. The choice of this threshold rather than using I lies in the fact that electronic excitations with threshold lower than I can occur below this value. Hence, we assume a gradually varying threshold as a function of energy around the I

https://dx.doi.org/10.1021/acs.jpca.0c02575
J. Phys. Chem. A 2020, 124, 5147−5156

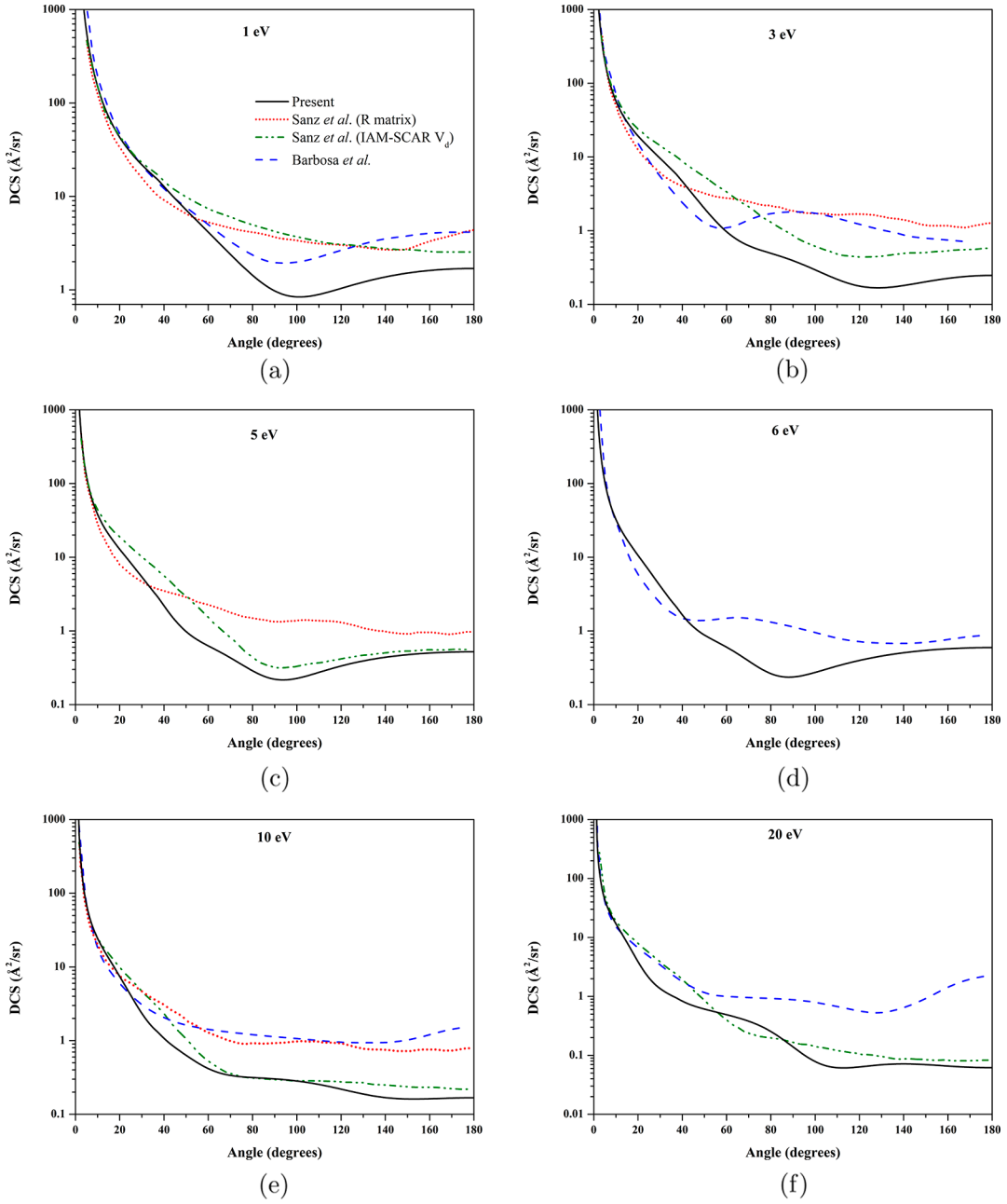

Figure 3. Differential cross-sections for pyrimidine. Solid line: present results, dotted line: *R*-matrix results of Sanz et al.,[20] dash-dot- dotted line: IAM-SCAR calculations with dipole potential of Sanz et al.[20] and dashed line: SMC results of Barbosa et al.[19]

of the target with a minimum value of the first allowed excitation energy of the target. This approximation is meaningful because Δ fixed at I would not allow low-energy excitations and high-energy inner shell ionizations. Now, R is determined by imposing boundary conditions.[24] This way, Q_{ion} can be extracted from Q_{in}. Once Q_{ion} is obtained, electronic excitation cross-section $Q_{elec,exc}$ can be easily computed. Besides, the difference between Q_{inel} and Q_{in} gives us the Ps formation cross-section (Q_{Ps}). Moreover, Ps formation also leads to an ionization channel because it leaves the target ionized. Thus, it is required to add this Q_{Ps} to Q_{ion} to get the total ionization cross-section $Q_{tot,ion}$.

Because the experimental data are summed for rotational and vibrational excitations, owing to the limited energy resolution of the beam, it becomes necessary to account for these effects for a reasonable comparison between theory and experiment. Here, we have adopted the Dickinson model[38] for rotational excitation, which follows the first born approximation at lower scattering angles and introduces a correction for medium and large angles. The final form for rotational DCS is given as,

For $\theta < \theta_c$

$$\frac{d\sigma^{Born}}{d\Omega} \approx \frac{D^2}{6E \sin^2\frac{\theta}{2}} \tag{9}$$

For $\theta \geq \theta_c$

$$\frac{d\sigma^{Dic}}{d\Omega} \approx \frac{\pi D}{64E \sin^3\frac{\theta}{2}} \tag{10}$$

https://dx.doi.org/10.1021/acs.jpca.0c02575
J. Phys. Chem. A 2020, 124, 5147−5156

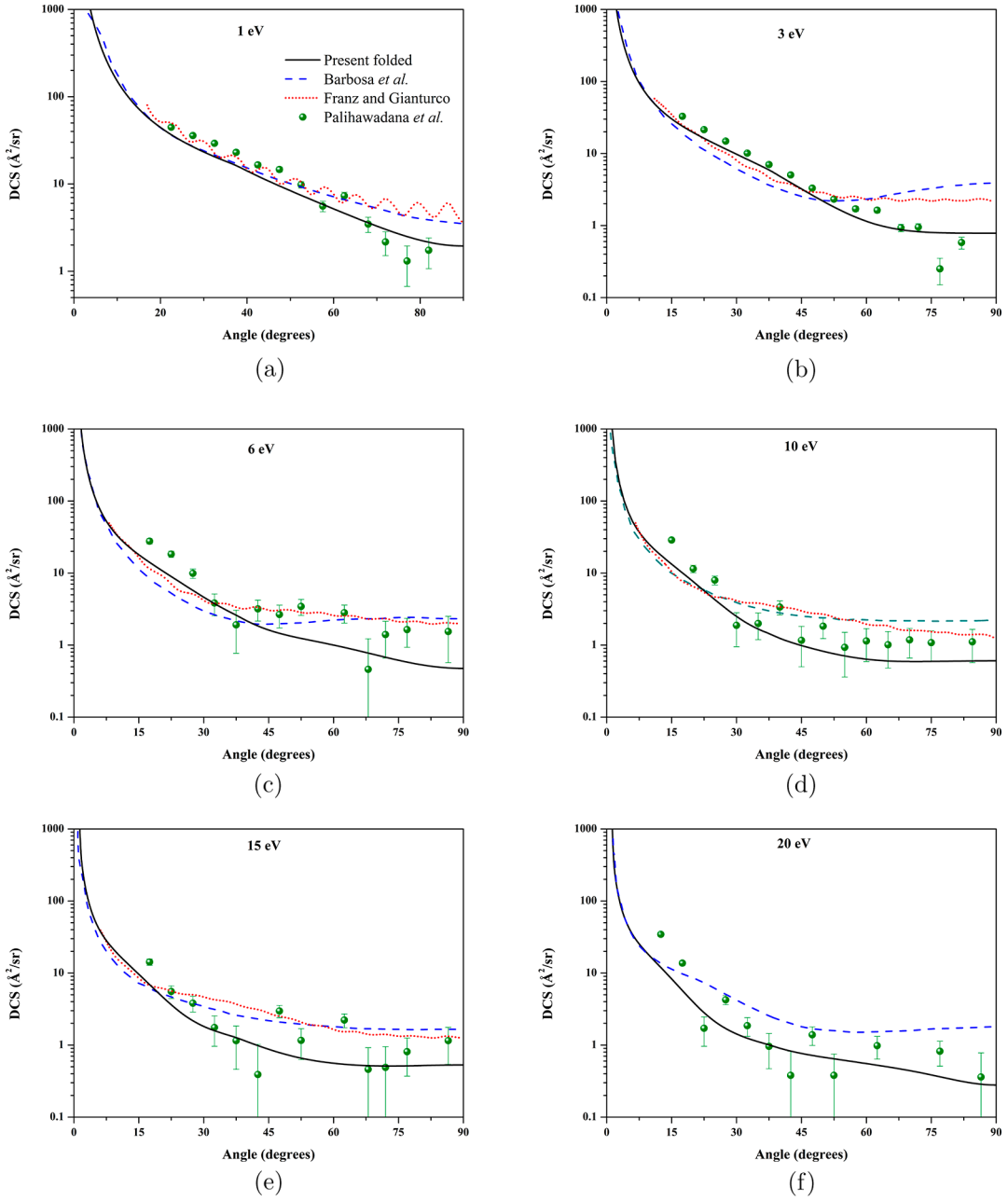

Figure 4. Folded differential cross-section for pyrimidine. Solid line: present results, dashed line: SMC results of Barbosa et al.,[19] dotted line: quantum mechanical calculations of Franz and Gianturco[21] and spheres: folded experimental data of Palihawadana et al.[17]

Here, D is the dipole moment and E is the incident energy. θ_c is the angle at which the two cross-sections intersect each other, which was found to be around 38° for the both targets. For molecules with a high dipole moment, as in the present case, this form of DCS gives a better representation of angular variation. This approach is the same as suggested by Blanco et al.[39] For the integral rotational excitation cross-section, authors have given an analytical expression

$$Q_{\mathrm{rot}} \approx \frac{4\pi D^2}{3E} \ln \frac{4E}{|\Delta E_{\mathrm{rot}}^{\mathrm{eff}}|} \tag{11}$$

Here, $\Delta E_{\mathrm{rot}}^{\mathrm{eff}}$ is the average excitation energy for the transition, which is around 1 meV for both the molecules. Similar calculations have already been performed for pyrimidine[16] and pyridine[22] and further details can be found from these references. Adding this Q_{rot} to the elastic and total cross-sections computed using SCOP-EPM gives us the rotationally summed elastic and grand total cross-sections, respectively.

RESULTS AND DISCUSSION

A comprehensive study of various cross-sections for positron impact scattering from pyrimidine and pyridine molecules is done and the results are presented graphically in Figures 3−11. By and large, very good agreement can be seen between the present results and the previous experimental data.

Differential Cross-Section. The elastic differential cross-section including the rotational contribution is presented here. For pyrimidine, the folded experimental DCS of Palihawadana et al.[17] is available. The theoretical cross-sections include the R-matrix and IAM-SCAR calculation of Sanz et al.[20] and SMC

https://dx.doi.org/10.1021/acs.jpca.0c02575
J. Phys. Chem. A 2020, 124, 5147−5156

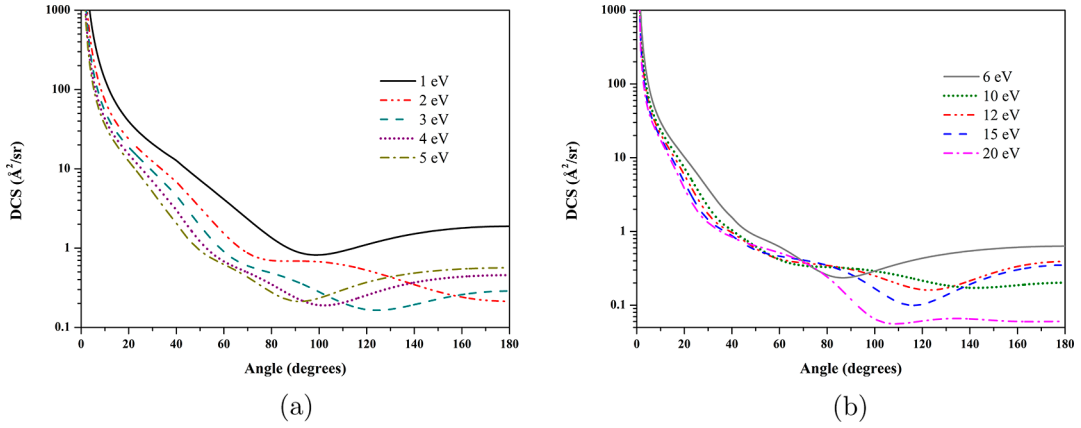

Figure 5. Present differential cross-section for pyridine at selected energies.

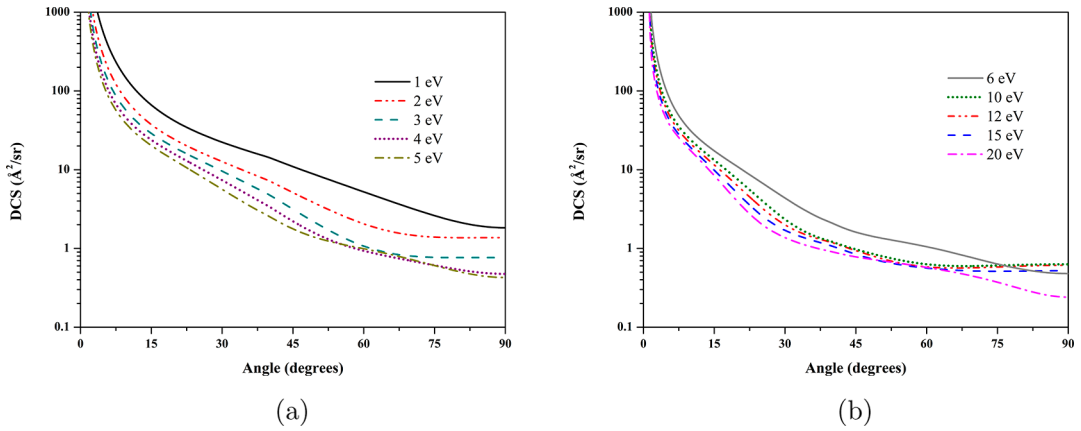

Figure 6. Present folded differential cross-section for pyridine at selected energies.

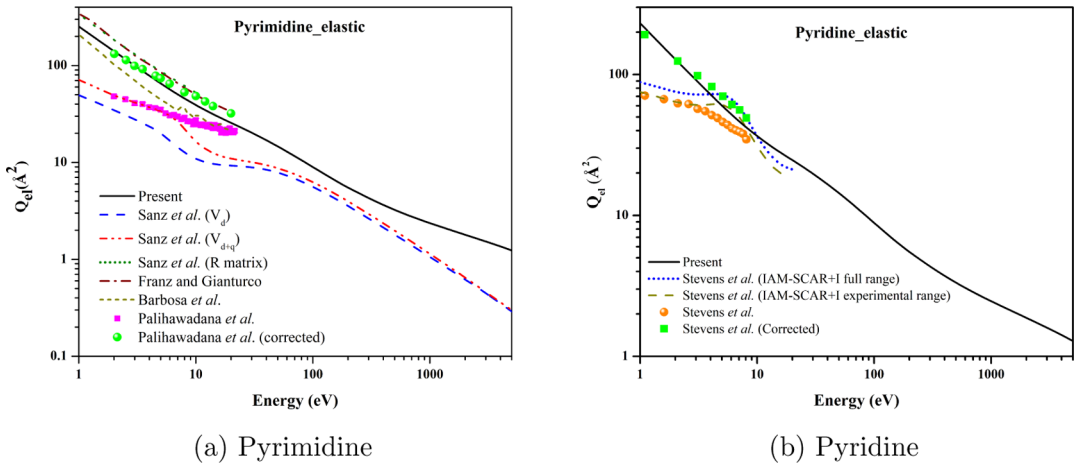

Figure 7. Elastic (rotationally summed) cross-section. (a) Solid line: present results, dashed line: IAM (V_d) results of Sanz et al.,[20] dashed-dot-dotted line: IAM (V_{d+q}) results of Sanz et al.,[20] dotted line: *R* matrix results of Sanz et al.,[20] dash-dotted line: Franz and Gianturco,[21] short-dashed line: SMC results of Barbosa et al.,[19] squares: experimental data of Palihawadana et al.[17] and spheres: forward-angle-corrected data of Palihawadana et al.[21] (b) Solid line: present results, dotted and dashed line: IAM-SCAR results of Stevens et al.,[22] spheres: experimental results of Stevens et al.[22] and squares: forward-angle-corrected data of Stevens et al.

cross-sections of Barbosa et al.[19] In Figure 3, present DCS along with other theoretical data is plotted. Except for 1 eV, the present results show good matching with the IAM-SCAR results of Sanz et al.[20] The authors have also reported the *R*-matrix cross-sections using SP and CC approximation. For brevity, we have included only the CC results in the comparison graph. The angular dependence is similar to the present cross-sections, except the magnitude, which is higher for the larger scattering angles. Furthermore, decent agreement with the SMC results of Barbosa et al.[19] can be seen at low and higher scattering angles. Because of the exclusion of the ionization and positronium formation channel in the *R*-matrix and SMC calculations, not only the magnitude, but also the structure varies from the present plot. As pointed by Barbosa et

https://dx.doi.org/10.1021/acs.jpca.0c02575
J. Phys. Chem. A 2020, 124, 5147−5156

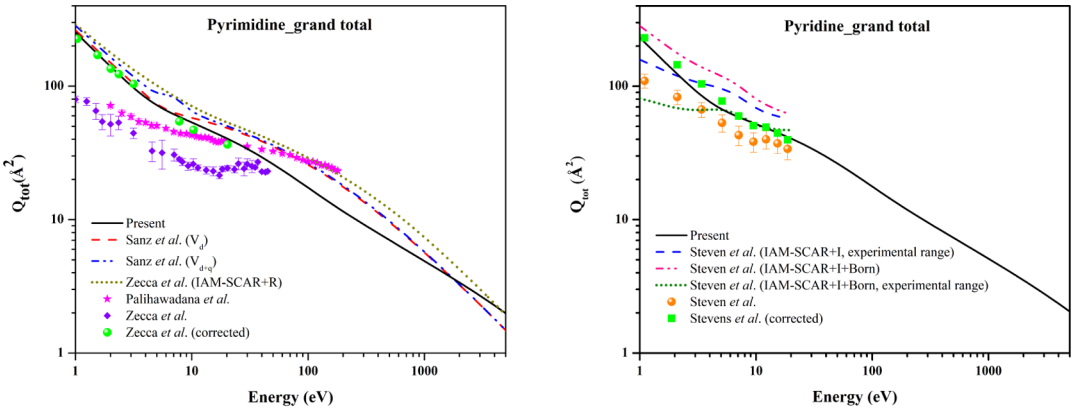

(a) Pyrimidine (b) Pyridine

Figure 8. Grand total cross-section. (a) Solid line: present results, dashed line: IAM (V_d) results of Sanz et al.,[20] dashed-dot-dotted line: IAM (V_{d+q}) results of Sanz et al.,[20] dotted line: IAM-SCAR+R results of Zecca et al.,[16] stars: experimental data of Palihawadana et al.,[17] squares: experimental measurements of Zecca et al.[16] spheres: forward-angle-corrected data of Zecca et al.[21] (b) Solid line: present results, dashed line: IAM-SCAR+I calculation for the experimental range of Stevens et al.,[22] dash-dot-dotted and dotted line: IAM-SCAR+I+Born results of Stevens et al.[22] for the full range and the experimental range, respectively, spheres: experimental results of Stevens et al.[22] and squares: forward-angle-corrected data of Stevens et al.

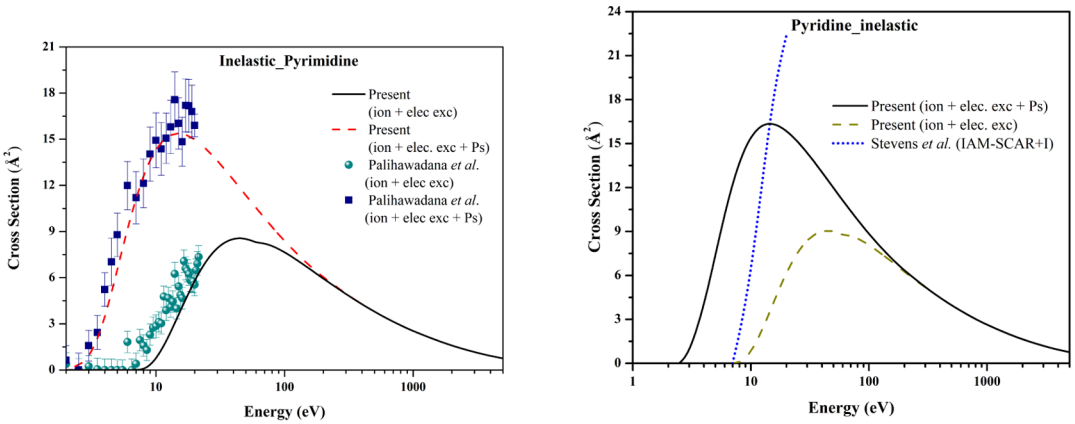

(a) Pyrimidine (b) Pyridine

Figure 9. Inelastic cross-section. Dashed line: present inelastic results excluding Ps formation, solid line: present inelastic cross-section including Ps formation. (a) Spheres: experimental data of Palihawadana et al.[17] excluding Ps, spheres: experimental data of Palihawadana et al.[17] including Ps. (b) Dotted line: IAM-SCAR cross-section of Stevens et al.[22]

al.,[19] these multichannel coupling effects reduce the elastic cross-sections. Nonetheless, the IAM-SCAR results include these important channels (though not very effectively) and hence show good agreement with the present results. In Figure 4, the folded results are shown. The data are compared to the experimental findings of Palihawadana et al.[17] and very good corroboration can be found. The theoretical cross-sections from Barbosa et al.[19] and Franz and Ginaturco[21] are also shown in the comparison plot. As can be seen, the present results lie within the experimental uncertainty of Palihawadana et al.[17] Furthermore, other two theoretical approaches produce higher cross-sections for large scattering angles and lower values for lower angles, when compared to the experiments. This is again because of the negligence of Ps formation and ionization channels in these computations. Nonetheless, the present results, in general, show good agreement with the measurements for the common comparative angles.

The present DCS for pyridine is shown in Figures 5 and 6. No previous data are available for comparison.

Elastic and Total Cross-Section. Figure 7 shows the elastic cross-section for pyrimidine and pyridine. For pyrimidine, Sanz et al.[20] have reported the IAM results that include dipole and quadrupole potentials (V_{d+q}). The V_{d+q} results are in good agreement with the experimental results of Palihawadana et al.[17] However, the experimental data are not corrected for forward-angle scattering, which has significant contribution in the low energy range. Though the modified data are reported by Franz and Gianturco[21] who used their theoretical values to find the missing contribution in the experiment. The cross-sections of Franz and Gianturco[21] show decent agreement with the corrected values; however, they are higher below the Ps formation threshold. This again may be because of the negligence of the inelastic channels in their calculations. The same explanation applies for the *R*-matrix results of Sanz et al.[20] which overlap with the findings of Franz

https://dx.doi.org/10.1021/acs.jpca.0c02575
J. Phys. Chem. A 2020, 124, 5147−5156

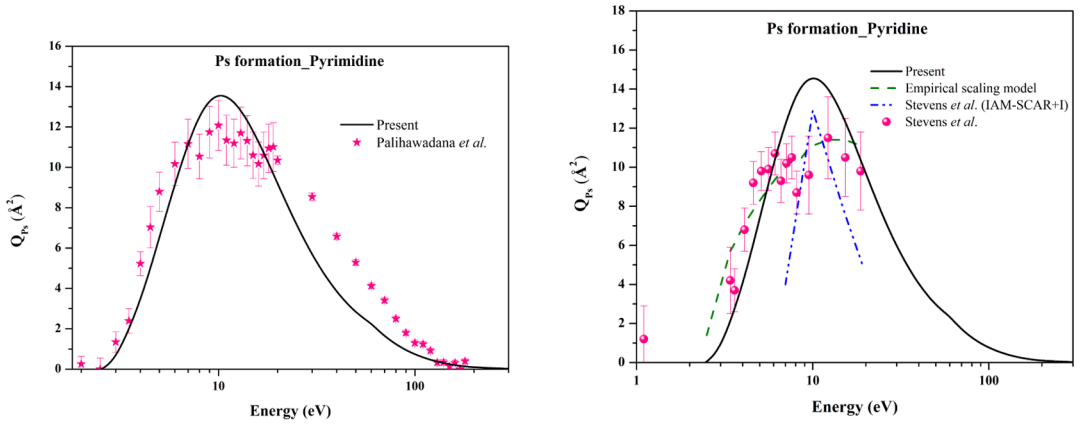

(a) Pyrimidine (b) Pyridine

Figure 10. Positronium formation cross-section. Solid line: present results. (a) Stars: experimental data of Palihawadana et al.,[17] (b) dashed line: results of Stevens et al.[22] computed using the empirical scaling factor, dash-dot-dotted line: IAM-SCAR cross-section of Stevens et al.,[22] spheres: experimental data of Stevens et al.[22]

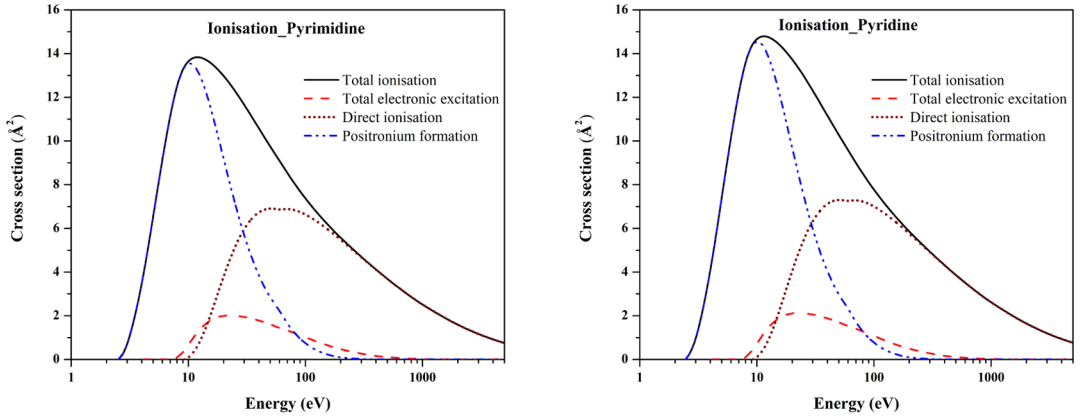

(a) Pyrimidine (b) Pyridine

Figure 11. Solid line: total ionization cross-section, dashed line: total electronic excitation cross-section, dotted line: direct ionization cross-section and dash-dot-dotted line: positronium formation cross-section.

and Gianturco. The present results show excellent agreement with the experimental cross-section.[17] The SMC results[19] are not dipole corrected and hence show deviation from other available data.

Present elastic cross-sections (including rotational excitations) for pyridine are shown in Figure 7b. There is only one experimental cross-section available.[22] Authors have also reported the IAM-SCAR including interference terms, which show decent agreement with the experimental data. However, the experimental setup cannot separate the rotational excitation contribution from the elastic ones and hence Q_{el} are rotationally summed. Furthermore, because of the limitation to cover the entire scattering angle, the experimental results lack the major contribution from forward-angle scattering. Hence, for a rational comparison, we used present DCS (eq 5) to find this contribution. The following part is added to obtain the corrected experimental cross-section.

$$\sigma_{\text{forward}} = 2\pi \int_0^{\theta_{\min}} \frac{d\sigma_{\text{cal}}}{d\Omega} \sin\theta \, d\theta \tag{12}$$

$\theta_{\min}$ is the critical angle below which the experimental setup cannot measure the elastic cross-section. In their article,[22] authors have provided this critical angle for selected energies. Because $\theta_{\min} \propto 1/\sqrt{E}$,[21] a minimum angle for any energy E can be determined. We have added this correction to the measured data for elastic and total cross-sections. The corrected experimental cross-sections and the present elastic data (rotationally summed) show very good agreement with each other. Furthermore, the rotational part needs to be added to the IAM results for a logical comparison. However, when we compared our elastic cross-sections (without rotational excitations), which is not shown here for brevity, we found that the IAM-SCAR values are higher than the present data. The IAM-SCAR approach basically adds the contributions from atomic constituents, without considering the molecular properties in the calculations. Furthermore, screening correction is carried out to improve the produced results. This approach produces reasonable results in the range ≥30 eV and is not suitable for low-energy investigation. Besides, present model includes molecular geometry throughout the codes and no other correction is required to induce the target structure in the computation. Thus, the present approach is finer than the IAM-SCAR method and the introduction of

https://dx.doi.org/10.1021/acs.jpca.0c02575
J. Phys. Chem. A 2020, 124, 5147−5156

EPM has further extended our credibility in the low-energy region as well.

The grand total cross-section (direct ionization + electronic excitation + rotational excitation + positronium formation + elastic) along with the available theoretical and experimental data is depicted in Figure 8. However, for clarity, we have not included the results, which do not include rotational excitation.[16,18] For pyrimidine, Palihawadana et al.[17] and Zecca et al.[16] have reported the experimental cross-sections. However, their data are raw and do not account for the forward-angle contribution. Similar to elastic cross-section, Sanz et al.[20] have provided the corrected data for Zecca et al.[16] Present results show excellent agreement with the corrected data. Besides, in the low-energy range, IAM-SACR+R cross-sections are higher than the present results, which is because of the limitation of the former approach in the low-energy range.

For pyridine, a noticeable difference can be seen among the available cross-sections. We added the forward-angle contribution as done for elastic cross-sections and found good agreement with the experimental results. The IAM-SCAR+I +Born result is significantly higher than the present and modified measurements, which again is because of the negligence of molecular geometry and inadequate way of dealing with the Ps formation channel in the low-energy range. Furthermore, more experiments and sophisticated theoretical calculations such as SMC and the *R*-matrix are needed to investigate this scattering system and bridge the gap between the existing data.

Inelastic Cross-Section. Figure 9 illustrates the inelastic cross-sections computed using the present approach. We have shown both with Ps (Q_{inel}) and without Ps (Q_{in}) results. Present Q_{in} shows fair agreement with the measured data of Palihawadana et al.[17] The authors have tabulated the Q_{in} and Q_{Ps} data in their article. We have added these data and determined the error propagated in these data to find the experimental Q_{inel}. Excellent agreement can be observed between the present and experimental data. For pyridine, the IAM results differ significantly from the present cross-sections. The approach is known to produce larger cross-sections in the low-energy range and only above 25−30 eV, reliable cross-sections can be obtained. Furthermore, the Ps threshold for respective atoms are used in their work instead of the molecule, which results in the right shifting of the curve when compared to the present results.

Positronium Formation Cross-Section. Figure 10 depicts the present positronium formation cross-section plotted with other comparisons. Present Q_{Ps} for pyrimidine shows very good agreement with the experimental data;[17] however, in the intermediate to high energy range, the present cross-section falls off steeply. Our results for pyridine show reasonable agreement with the experimental results and the peak energy matches well with the experimental and theoretical data of Stevens et al.[22] The scaling model gives good estimate of the Ps cross-section. Moreover, the IAM-SCAR+I model fails to reproduce the experimental trend. Besides, it is well known that the Ps formation channel fades away at energies ∼100−200 eV, which is the case shown in the graph. As the energy reaches 200 eV, the Ps channel finally disappears from the scattering process.

Ionization Cross-Section. A graphical illustration of various inelastic channels is shown in Figure 11. The sum total of all electronic excitation cross-sections is also shown along with it. The general feature of the inelastic/ionization process can be clearly seen where the cross-sections initially increase and after attaining a peak value start falling off. Other theoretical attempts and experiments are needed to substantiate the present results.

CONCLUSION

SCOP-EPM cross-sections for a range of processes are reported in this article. Very good agreement was found between the present results and the experimental data.[16,17,22] For the positronium formation cross-section, a decent match is obtained and the position at peak energy matches well with the experimental results.[17,22] Total electronic excitation and direct and total ionization cross-sections are reported here for the first time. For DCS, the present results for pyrimidine are in better agreement, when compared with other theoretical models. This asks for proper inclusion of inelastic channels in any theoretical approach. For pyridine, no comparison is available and experiments are needed to support the present findings. By including the EPM to the SCOP, substantially improved results are obtained. We look forward to experiments for more rigorous check to the present calculations.

AUTHOR INFORMATION

Corresponding Author

Bobby Antony − *Atomic and Molecular Physics Lab, Department of Physics, Indian Institute of Technology (Indian School of Mines) Dhanbad, Dhanbad, Jharkhand 826004, India;* orcid.org/0000-0003-2073-9681; Email: bobby@iitism.ac.in

Authors

Nidhi Sinha − *Atomic and Molecular Physics Lab, Department of Physics, Indian Institute of Technology (Indian School of Mines) Dhanbad, Dhanbad, Jharkhand 826004, India*

Aloka Kumar Sahoo − *Department of Physics, Indian Institute of Technology Roorkee, Roorkee, Uttarakhand 247667, India*

Complete contact information is available at: https://pubs.acs.org/10.1021/acs.jpca.0c02575

Notes

The authors declare no competing financial interest.

The data that support the findings of this study are available from the corresponding author upon reasonable request.

ACKNOWLEDGMENTS

Authors are thankful to J. Sullivan (Australian National University) for constructive discussion on their experimental measurements on pyridine. B.A. is pleased to acknowledge the support of this research by the Department of Science and Technology, Govt of India through SERB project grant no. EMR/2016/005035.

REFERENCES

(1) Hamada, Y. *Pyridine*; IntechOpen, 2018.

(2) Katoh, A.; Hashimoto, T. Molecular Biology of Pyridine Nucleotide and Nicotine Biosynthesis. *Front. Biosci.* **2004**, *9*, 1577−1586.

(3) Nakamura, M.; Bhatnagar, A.; Sadoshima, J. Overview of Pyridine Nucleotides Review Series. *Circ. Res.* **2012**, *111*, 604−610.

(4) Altaf, A. A.; Shahzad, A.; Gul, Z.; Khan, S. A.; Badshah, A.; Tahir, M. N.; Zafar, Z. I.; Khan, E. A Review on the Medicinal Importance of Pyridine Derivatives. *J. Drug Des. Med. Chem.* **2015**, *1*, 1−11.

(5) Braun, R.; Schaper, W.; Stark, H.; Preuss, R.; Knauf, W.; Sanft, U.; Kern, M.; Bonin, W. Substituted Pyridines/Pyrimidines, Their Preparation and Their Use as Pesticides. U.S. Patent 6,265,398 B1, 2001.
(6) Guan, A.-Y.; Liu, C.-L.; Sun, X.-F.; Xie, Y.; Wang, M.-A. Discovery of Pyridine-Based Agrochemicals by Using Intermediate Derivatization Methods. *Bioorg. Med. Chem.* **2016**, *24*, 342−353.
(7) Smith, K. E.; Callahan, M. P.; Gerakines, P. A.; Dworkin, J. P.; House, C. H. Investigation of Pyridine Carboxylic Acids in CM2 Carbonaceous Chondrites: Potential Precursor Molecules for Ancient Coenzymes. *Geochim. Cosmochim. Acta* **2014**, *136*, 1−12.
(8) Sephton, M. A. Organic Compounds in Carbonaceous Meteorites. *Nat. Prod. Rep.* **2002**, *19*, 292−311.
(9) Parker, D. S. N.; Kaiser, R. I.; Kostko, O.; Troy, T. P.; Ahmed, M.; Sun, B.-J.; Chen, S.-H.; Chang, A. H. H. On the Formation of Pyridine in the Interstellar Medium. *Phys. Chem. Chem. Phys.* **2015**, *17*, 32000−32008.
(10) Phelps, M. E. Positron Emission Tomography Provides Molecular Imaging of Biological Processes. *Proc. Natl. Acad. Sci. U.S.A.* **2000**, *97*, 9226−9233.
(11) Jan, S.; Santin, G.; Strul, D.; Staelens, S.; Assié, K.; Autret, D.; Avner, S.; Barbier, R.; Bardiès, M.; Bloomfield, P. M.; et al. GATE: A Simulation Toolkit for PET and SPECT. *Phys. Med. Biol.* **2004**, *49*, 4543.
(12) Blanco, F.; Munoz, A.; Almeida, D.; da Silva, F. F.; Limao-Vieira, P.; Fuss, M. C.; Sanz, A. G.; García, G. Modelling Low Energy Electron and Positron Tracks in Biologically Relevant Media. *Eur. Phys. J. D* **2013**, *67*, 199.
(13) Fuss, M. C.; Ellis-Gibbings, L.; Jones, D. B.; Brunger, M. J.; Blanco, F.; Muñoz, A.; Limão-Vieira, P.; García, G. The Role of Pyrimidine and Water as Underlying Molecular Constituents for Describing Radiation Damage in Living Tissue: A Comparative Study. *J. Appl. Physiol.* **2015**, *117*, 214701.
(14) Rubin, C. M.; Schmid, C. W. Pyrimidine-Specific Chemical Reactions Useful for DNA Sequencing. *Nucleic Acids Res.* **1980**, *8*, 4613−4620.
(15) Arce, P.; Muñoz, A.; Moraleda, M.; Ros, J. M. G.; Blanco, F.; Perez, J. M.; García, G. Integration of the Low-Energy Particle Track Simulation Code in Geant4. *Eur. Phys. J. D* **2015**, *69*, 188.
(16) Zecca, A.; Chiari, L.; García, G.; Blanco, F.; Trainotti, E.; Brunger, M. J. Total Cross Sections for Positron and Electron Scattering from Pyrimidine. *J. Phys. B: At., Mol. Opt. Phys.* **2010**, *43*, 215204.
(17) Palihawadana, P.; Boadle, R.; Chiari, L.; Anderson, E.; Machacek, J.; Brunger, M. J.; Buckman, S.; Sullivan, J. Positron Scattering from Pyrimidine. *Phys. Rev. A: At., Mol., Opt. Phys.* **2013**, *88*, 012717.
(18) Sinha, N.; Antony, B. Electron and Positron Interaction with Pyrimidine: A Theoretical Investigation. *J. Appl. Physiol.* **2018**, *123*, 124906.
(19) Barbosa, A. S.; Pastega, D. F.; Bettega, M. H. F. Low-Energy Positron Scattering by Pyrimidine. *J. Chem. Phys.* **2015**, *143*, 244316.
(20) Sanz, A. G.; Fuss, M.; Blanco, F.; Mašín, Z.; Gorfinkiel, J.; McEachran, R.; Brunger, M. J.; Garcia, G. Cross-Section Calculations for Positron Scattering from Pyrimidine Over an Energy Range from 0.1 to 10000 eV. *Phys. Rev. A: At., Mol., Opt. Phys.* **2013**, *88*, 062704.
(21) Franz, J.; Gianturco, F. Low-Energy Positron Scattering from Gas-Phase Pyrimidine: A Quantum Treatment of the Dynamics and a Comparison with Experiments. *Phys. Rev. A: At., Mol., Opt. Phys.* **2013**, *88*, 042711.
(22) Stevens, D.; Babij, T. J.; Machacek, J. R.; Buckman, S. J.; Brunger, M. J.; White, R. D.; García, G.; Blanco, F.; Ellis-Gibbings, L.; Sullivan, J. P. Positron Scattering from Pyridine. *J. Chem. Phys.* **2018**, *148*, 144308.
(23) Antony, B. K.; Joshipura, K. N.; Mason, N. J. Total and Ionization Cross Sections of Electron Scattering by Fluorocarbons. *J. Phys. B: At., Mol. Opt. Phys.* **2005**, *38*, 189.
(24) Sinha, N.; Modak, P.; Singh, S.; Antony, B. Positron Scattering from Methyl Halides. *J. Phys. Chem. A* **2018**, *122*, 2513−2522.
(25) Salvat, F.; Martnez, J. D.; Mayol, R.; Parellada, J. Analytical Dirac-Hartree-Fock-Slater screening function for atoms (Z= 1−92). *Phys. Rev. A: At., Mol., Opt. Phys.* **1987**, *36*, 467.
(26) Watson, G. *A Treatise on the Theory of Bessel Functions*; Cambridge University Press, 1958.
(27) Zhang, X.; Sun, J.; Liu, Y. A New Approach to the Correlation Polarization Potential-Low-Energy Electron Elastic Scattering by He Atoms. *J. Phys. B: At., Mol. Opt. Phys.* **1992**, *25*, 1893.
(28) Perdew, J. P.; Zunger, A. Self-Interaction Correction to Density-Functional Approximations for Many-Electron Systems. *Phys. Rev. B: Condens. Matter Mater. Phys.* **1981**, *23*, 5048−5079.
(29) Jain, A. Low-energy positron-argon collisions by using parameter-free positron correlation polarization potentials. *Phys. Rev. A: At., Mol., Opt. Phys.* **1990**, *41*, 2437−2444.
(30) Staszewska, G.; Schwenke, D. W.; Truhlar, D. G. Investigation of the Shape of the Imaginary Part of the Optical-Model Potential for Electron Scattering by Rare Gases. *Phys. Rev. A: At., Mol., Opt. Phys.* **1984**, *29*, 3078−3091.
(31) Blanco, F.; García, G. Improved Non-Empirical Absorption Potential for Electron Scattering at Intermediate and High Energies: 30−10000 eV. *Phys. Lett. A* **1999**, *255*, 147−153.
(32) Chiari, L.; Zecca, A.; Girardi, S.; Trainotti, E.; García, G.; Blanco, F.; McEachran, R. P.; Brunger, M. J. Positron Scattering from O_2. *J. Phys. B: At., Mol. Opt. Phys.* **2012**, *45*, 215206.
(33) CCCBDB, Computational Chemistry Comparison and Benchmark DataBase. https://cccbdb.nist.gov/ (accessed December 10, 2019).
(34) Mašín, Z.; Gorfinkiel, J. D.; Jones, D. B.; Bellm, S. M.; Brunger, M. J. Elastic and Inelastic Cross Sections for Low-Energy Electron Collisions with Pyrimidine. *J. Chem. Phys.* **2012**, *136*, 144310.
(35) Bauernschmitt, R.; Ahlrichs, R. Treatment of Electronic Excitations Within the Adiabatic Approximation of Time Dependent Density Functional Theory. *Chem. Phys. Lett.* **1996**, *256*, 454−464.
(36) Walker, I. C.; Palmer, M. H.; Hopkirk, A. The Electronic States of the Azines. II. Pyridine, Studied by VUV Absorption, Near-Threshold Electron Energy Loss Spectroscopy and Ab Initio Multi-Reference Configuration Interaction Calculations. *Chem. Phys.* **1990**, *141*, 365−378.
(37) Hanwell, M. D.; Curtis, D. E.; Lonie, D. C.; Vandermeersch, T.; Zurek, E.; Hutchison, G. R. Avogadro: An Advanced Semantic Chemical Editor, Visualization, and Analysis Platform. *J. Cheminf.* **2012**, *4*, 17.
(38) Dickinson, A. S. Differential Cross Sections for Electron Scattering by Strongly Polar Molecules. *J. Phys. B: At. Mol. Phys.* **1977**, *10*, 967.
(39) Blanco, F.; Muñoz, A.; Almeida, D.; Silva, F. F. d.; Limão-Vieira, P.; García, G. Clustering and Condensation Effects in the Electron Scattering Cross Sections from Water Molecules. *Int. J. Mass Spec.* **2014**, *365−366*, 287−294.

https://dx.doi.org/10.1021/acs.jpca.0c02575
J. Phys. Chem. A 2020, 124, 5147−5156